International Journal of Engineering Inventions
e-ISSN: 2278-7461, p-ISSN: 2319-6491
Volume 14, Issue 5 [May. 2025] PP: 120-125

Research on the Pattern of Stress Distribution on Displacement Fluctuation in Train Door Belt Transmission System

YaoChenShi[a], EnQuanChang[a], YiChen[b], ShuAnQin[c], Peng Zhou[c]
[a]*College of Mechanical and Vehicular Engineering, Changchun University, Changchun 130022, China*
[b]*Zhejiang Sante Technology Co., Ltd, Taizhou 318000, China*
[c]*China Machinery Productivity Promotion Center Co., Ltd, Beijing 100044, China*
Corresponding Author: WushengTang

Abstract: *To investigate the influence mechanism of stress distribution on displacement fluctuations in train door belt drive systems, a rigid-flexible coupling dynamic model was established for comprehensive simulation analysis. Comparative analysis between displacement oscillation characteristics and stress distribution curves revealed the intrinsic correlation governing stress-displacement interactions. Experimental validation was conducted to verify the simulation reliability through purpose-built test apparatus. The investigation yielded three principal findings: (1) X-direction displacement fluctuations predominantly concentrate in the span region with amplitude amplification proportional to belt elongation; (2) Reduced displacement amplitudes in contact zones are attributed to the synergistic effects of contact stress, bending stress, and tensile stress enhancing belt-idler conformity; (3) Diminished fluctuation magnitudes in meshing zones result from elevated meshing stresses intensifying interfacial contact integrity between belt teeth and pulley teeth.*

Key Words*: Train door, Belt; drive, Displacement fluctuation, Stress*

Date of Submission: 10-05-2025 Date of acceptance: 20-05-2025

I. Introduction

The rapid urbanization and exponential expansion of rail transit systems have established trains as an imperative transportation modality in modern society [1-2]. The belt drive system of train doors constitutes a critical safety component for passenger protection. This transmission mechanism has been widely adopted in industrial applications owing to its inherent advantages including structural simplicity, operational efficiency, robust stability, and cost-effective maintenance.

To further investigate the kinematic performance of belt drive systems, domestic and international scholars have primarily focused on dynamic modeling, stress distribution, and error analysis. Chen Hongyue et al. analyzed conveyor belt stress through experimental and numerical simulations [3]. Cao Zhongliang identified that increases in tension, pulley speed, and load lead to elevated belt stress [4]. Addressing system vibration issues, Wang Zhengjie et al. investigated intermittent motion and recommended tensioning pulleys to enhance precision [5]. Jozef Mascenik studied load conditions, revealing that velocity exerts the most significant influence on vibration, while appropriate tension-speed combinations can prolong belt lifespan [6]. Jiang Shaowei's analysis of force fluctuations demonstrated that a 90° angle minimizes impact effects [7]. For precision improvement, Ren Jihua et al. modified belt tooth profiles from linear to curved configurations, achieving enhanced positioning accuracy [8]. Kagotani's investigation of eccentric pulley effects indicated that tension adjustments effectively reduce resonance-induced errors [9]. Xian-bing BIAN proposed a "polygonal effect" model, demonstrating that increasing tooth count and reducing structural parameters enable smoother power transmission [10]. However, existing research exhibits a systematic deficiency in investigating the stress-displacement relationship within train door belt systems. This study establishes a rigid-flexible coupling model to analyze X-direction displacement fluctuations and stress distribution patterns, with experimental validation providing theoretical foundations for system optimization.

II. Establishment Of Train Door Belt Transmission System Model

2.1 Establishment of the Three-Dimensional Model

The three-dimensional computational model of the train door belt transmission system was systematically constructed in SolidWorks, as schematically depicted in Figure 1. The parametric assembly architecture consists of the following optimized components: (1) left door assembly, (2) slave pulley A, (3) reinforced support plate, (4) tensioner pulley A, (5) prime mover pulley, (6) tensioner pulley B, (7) slave pulley B, (8) high-precision synchronous belt, (9) interlocking connection plate, and (10) right door assembly. The established kinematic chain achieves bidirectional door operation through coordinated belt-pulley interaction, where rotational energy transmission from the prime mover induces anti-phase displacement of bilateral door modules via geometrically constrained belt routing, thus realizing deterministic door kinematics.

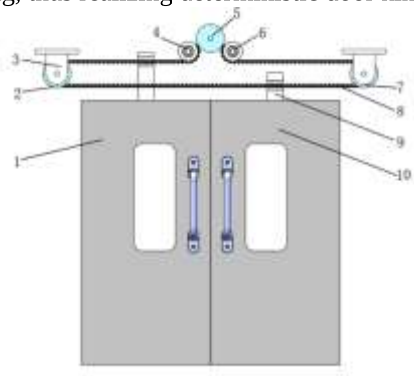

Fig.1 Train door belt drive system model

2.2 Establishment of Rigid-Flexible Coupled Dynamics Simulation Model

To improve simulation efficiency and reduce computation time, the train door belt transmission system model was simplified. Only key components were retained, including the synchronous belt, pulleys, and idler wheels. The door load was equivalent to a torque applied to the pulleys. Based on the trapezoidal tooth profile of the L-type synchronous belt, a three-dimensional model was established, where the synchronous belt has 148 teeth, a width of 20 mm, the pulley has 20 teeth, and the idler wheel diameter is 40 mm. The synchronous belt was treated as flexible, generating a mesh containing 28,300 elements and 45,240 nodes. To simplify the analysis, the synchronous belt was considered as a homogeneous material with a density of 1.26×10^3 kg/m³, elastic modulus of 2000 MPa, and Poisson's ratio of 0.47. The contact between pulleys, idler wheels, and the synchronous belt was set as rigid-flexible contact, and the simulation model is shown in Fig 2(a).

III. Simulation Analysis

3.1Rigid-Flexible Coupled Dynamics Analysis Process

For ease of modeling, the synchronous belt was simplified as a circular model and used as the initial simulation position, as shown in Fig 2(a). The idler wheels A and B were moved to the specified positions through a Step function, followed by adjustment of the positions of driven wheels A and B, setting the center distance to 546.81 mm to ensure that the synchronous belt tension force was 300 N, as shown in Fig 2(b). After the system remained stationary for 1 s, the drive wheel was driven to rotate counterclockwise at a uniform speed of 20 r/min through a Step function, while applying a torque of 2000 N·mm as shown in Fig 2(c). The total simulation time was set to 50 s with a time step of 5000.

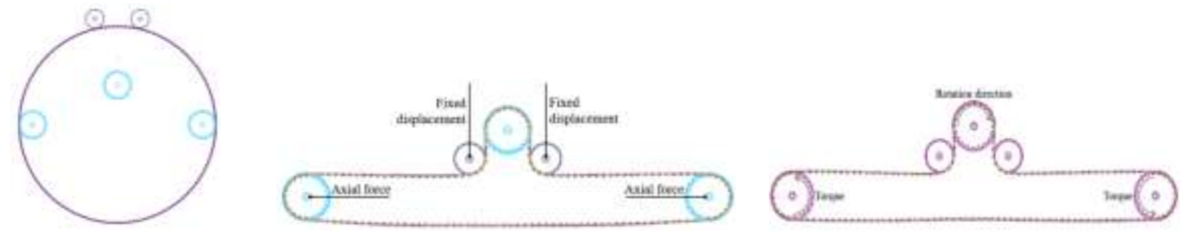

(a) Initial simulation position **(b) Application of fixed displacement and axial load** **(c) Apply rotational speed to the driving wheel,and torque to the driven wheel**

Fig.2 Rigid-flexible coupling dynamics analysis process

3.2Stress Cloud Diagram Analysis

The stress cloud diagram of the synchronous belt during the transmission process is shown in Fig 3. According to the motion characteristics, it is divided into three regions: In the span area sections JA, DE, FG, HI, and BC, the belt exhibits linear motion, with the belt body mainly subjected to tensile stress, the belt teeth experiencing almost no force, and stress concentrating at the connection between the belt teeth and belt body; In the contact area sections EF and IJ, the belt exhibits arc motion, with the belt body mainly subjected to the combined action of bending stress and contact stress, the belt teeth mainly experiencing bending stress, and stress concentrating on the belt back; In the meshing area sections AB, CD, and GH, the belt exhibits arc motion, with the belt body mainly subjected to bending stress and tensile stress, the tooth face mainly experiencing contact stress, and stress concentrating at the tooth root. To study the pattern of stress on displacement fluctuation, nodes

25562 at the midpoint of the belt back and 25554 at the midpoint of the belt tooth oblique edge were selected for analysis, and the displacement fluctuations in various regions were compared and verified.

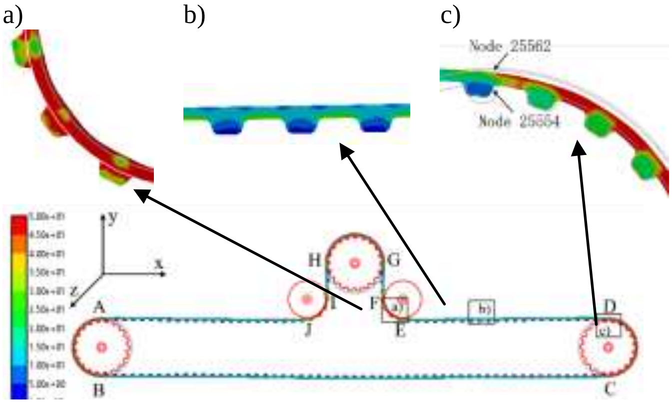

Fig.3 Stress contour map of the synchronous belt during the transmission process

3.3 Analysis of Stress and Displacement Fluctuation

Since the displacement change of nodes in the z direction is much smaller than in the x and y directions, and has little impact on the overall motion, only the displacement changes in the plane are analyzed. As shown in Fig 4, the motion of nodes in the x-y plane can be divided into three stages: the synchronous belt deployment and stop stage from 0-1s, the drive wheel acceleration stage from 1-1.2s, and the periodic motion stage after 1.2s. Taking the meshing position of the driven wheel as the starting point of the cycle, the period of the belt back node 25562 and the belt tooth node 25554 is 22.2s. Based on the simulation model and wheel system dimensions, a theoretical displacement curve was established. Using a time step of 0.01s, this curve was discretized to obtain 2220 sampling points, resulting in theoretical x and y direction displacement versus time curves. The same method was applied to establish theoretical displacement for the belt tooth node. Figure 5 shows the comparison between simulation and theoretical displacements of the belt back node 25562. After dividing the motion regions according to the movement characteristics in the x and y directions, it was found that the overall change trends between the two are consistent, verifying the rationality of the theoretical displacement model.

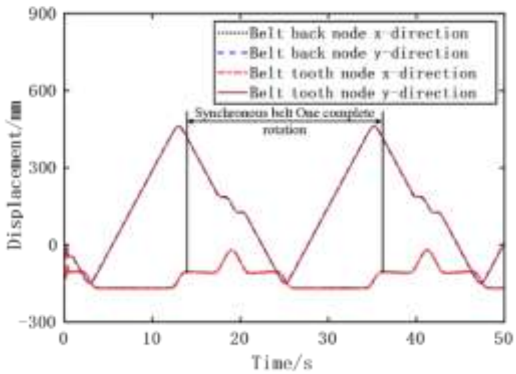

Fig.4 The x and y displacement curves of the nodes

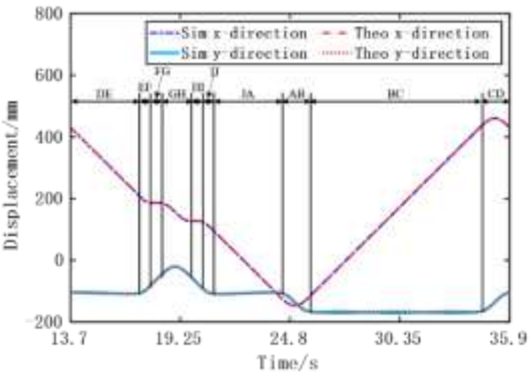

Fig.5 Comparison between belt-back simulation and theoretical displacement

The x-direction displacement is the main factor affecting the opening and closing of train doors, so only the displacement fluctuation in the x-direction is analyzed. By calculating the difference between the theoretical displacement and the simulation displacement in the x-direction, the displacement fluctuation of the node in the x-direction was obtained. The comparison between stress and x-direction displacement fluctuation of the belt back node 25562 is shown in Fig 6. From the figure, it can be seen that the displacement fluctuation is mainly concentrated in the span area, while the meshing area and contact area have smaller displacement fluctuations. This is because the span area is under tensile stress with weaker constraints, higher degrees of freedom, and is prone to larger displacement fluctuations; while the meshing area and contact area have concentrated stress due to contact action, resulting in smaller displacement fluctuations. The stresses in span area sections JA, BC, and DE are 8.75 MPa, 9.05 MPa, and 9.25 MPa, respectively, corresponding to displacement fluctuation amplitudes of 0.183 mm, 0.271 mm, and 0.186 mm. The displacement fluctuation amplitudes of sections JA and DE are basically consistent. As the belt length increases, under the same tensile stress, the longitudinal stiffness of the synchronous belt decreases, leading to an increase in displacement fluctuation amplitude. The maximum stress in the meshing area section AB is 109.61 MPa, with a peak-to-peak displacement fluctuation value of 0.093 mm, which is smaller than that in the span area. Since the belt back and belt body form an integral structure, the bending stress and contact stress generated when the belt body wraps around the pulley cause tight contact with the pulley, reducing the relative sliding between the belt body and the pulley, thus lowering the displacement fluctuation amplitude. The peak stress in the contact area section EF is 66.67 MPa, with a displacement fluctuation amplitude of 0.037 mm, which is smaller than that in the span area. When the belt back wraps around the idler wheel, bending stress and contact stress are generated, which together cause the belt to tightly adhere to the idler wheel, reducing the displacement fluctuation amplitude.

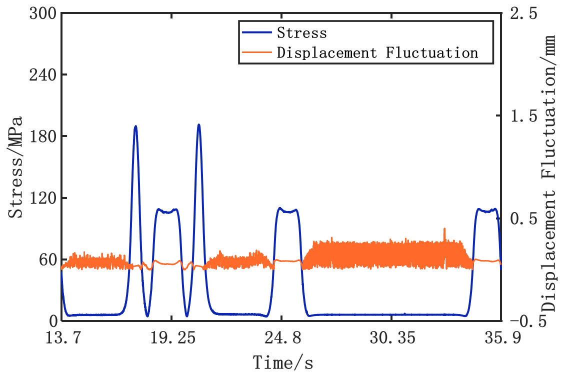

Fig.6 Comparison diagram of belt-back node stress and x-direction displacement fluctuation

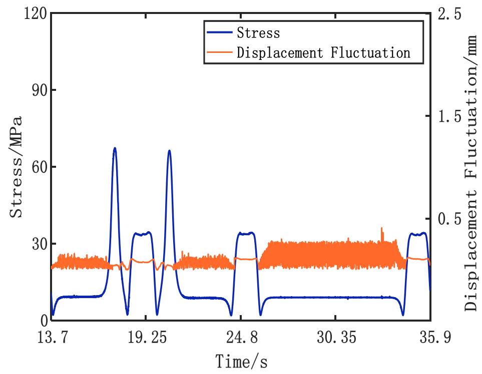

Fig.7 Comparison diagram of belt teeth node stress and x-direction displacement fluctuation

The comparison between stress and displacement fluctuation of the belt tooth node 25554 is shown in Fig 7. The stress amplitudes in the span area sections JA, BC, and DE are 8.75 MPa, 9.05 MPa, and 9.25 MPa, respectively, corresponding to displacement fluctuation amplitudes of 0.183 mm, 0.271 mm, and 0.186 mm. The displacement amplitude fluctuation in the belt tooth span area follows basically the same pattern as that of the belt back node. This is because the belt tooth and belt back form an integral structure. The maximum stress in the meshing area section AB is 34.2 MPa, with a peak-to-peak displacement fluctuation value of 0.098 mm, which is smaller than that in the span area. This is due to the meshing stress causing tight contact between the belt teeth and wheel teeth, reducing the displacement fluctuation amplitude. The peak stress of the belt tooth node in the contact area section EF is 66.67 MPa, with a displacement fluctuation amplitude of 0.045 mm. The displacement fluctuation amplitude is smaller compared to the span area, as the belt tooth and belt back form an integral structure, and under the action of contact stress and bending stress, the displacement fluctuation amplitude is reduced.

IV. Experimental Verification

4.1 Experimental Setup

To verify the accuracy of the simulation model, a two-pulley experimental setup was constructed as shown in Figure 8. The experimental setup consists of the following parts: a stepper motor drive system, a synchronous belt transmission system, a displacement measurement system, and a load system. The displacement measurement uses a GSCDA1000 type grating ruler to measure the x-direction displacement, which has a stroke of 1000 mm and a resolution of 5μm. The experiment uses an L-type synchronous belt with 121 teeth, a width of 20 mm, and 20 teeth on the pulley. After applying a 300 N tension force, the driven shaft seat is fixed, and a 10 kg load is applied. The drive wheel rotates in a clockwise direction, and the starting position for measurement is selected at the point where the synchronous belt disengages from the driven wheel, corresponding to the position of the belt back node 25562 in the simulation.

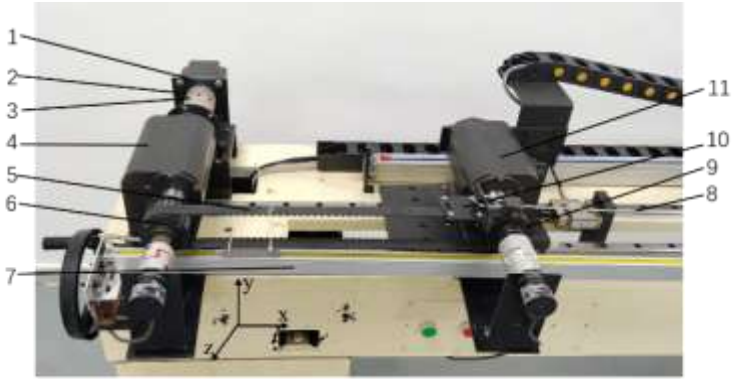

1 Stepper motor 2 Motor bracket 3 Coupling A 4 Drive shaft seat5 Synchronous belt 6 Drive wheel 7 Grating ruler 8 Load wire rope 9 Driven wheel10 Load fixing plate 11 Driven shaft seat
Fig.8 Displacement measurement device

4.2Comparison of Simulation and Experimental Results

To calculate the x-direction displacement fluctuation, the difference between the theoretical displacement and the actual displacement is defined:

$$\Delta d = |x_{theo} - x_{act}|$$

The calculation formula for the theoretical x-direction displacement is:

$$x_{theo} = \frac{\theta}{360} \times z \times p$$

Where:θ is the rotation angle of the drive wheel, in degrees; z is the number of teeth; p is the pitch, in mm.

To verify the simulation results, measurements were conducted under operating conditions at a speed of 20 r/min. The experimental x-direction displacement fluctuation curve was obtained by calculating the difference between the theoretical displacement and the actual measured displacement, and was compared with the x-direction displacement fluctuation of the belt back node 25562 in the DE section during the 14-16s time range in the simulation. The results are shown in Fig 9. The x-direction displacement fluctuation amplitudes of the experiment and simulation are 0.180 mm and 0.186 mm respectively, with a relative error of 3.33%. The simulation model basically reflects the displacement fluctuation pattern of the actual train door belt transmission system. The differences between the simulation and experimental results mainly stem from factors such as the tooth profile machining errors between the pulley teeth and belt teeth, the rotational accuracy of the pulley shaft system, and system vibrations during the experiment.

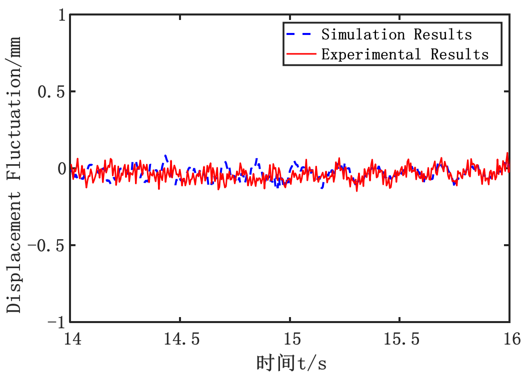

Fig.9 Comparison of x-direction displacement fluctuation between simulation and experiment

V. Conclusions

Through simulation and experimental studies of the stress distribution and displacement fluctuation in the train door belt transmission system, this paper has reached the following conclusions:
(1) In the train door belt transmission system, the x-direction displacement of the belt is parallel to the movement direction of the train door, directly affecting the opening and closing of the train door.
(2) The x-direction displacement fluctuation in the train door belt transmission system is mainly concentrated in the span area, while the amplitude of displacement fluctuation in the meshing area and contact area is smaller.

The span area is subjected only to tensile stress, resulting in weaker constraints and higher degrees of freedom; in comparison, the meshing stress in the meshing area causes tighter contact between the belt teeth and wheel teeth, reducing the amplitude of displacement fluctuation. In the contact area, the combined action of bending stress, contact stress, and tensile stress causes the belt to tightly adhere to the idler wheel, lowering the amplitude of displacement fluctuation.
(3) In the span area under the same tensile stress, as the belt length increases, the longitudinal stiffness decreases, significantly increasing the amplitude of displacement fluctuation.
(4) The relative error between the experimental displacement fluctuation and the simulation displacement fluctuation is 3.33%, indicating good consistency between the two and validating the simulation analysis.

Acknowledgement

This research was supported by the Jilin Provincial Natural Science Foundation (Provincial-Local Joint Fund-Changchun Innovation Development Joint Fund) project "Research on Fault Diagnosis Methods and Experimental Devices for Synchronous Belt Drive Systems Based on Multi-Signal Fusion" (Project No.: YDZJ202401325ZYTS).

References

[1]. Long Jing, Gao Wenming, Miao Xiaodong, et al. Overview of Urban Rail Transit Vehicle Door Technology [J]. Modern Urban Rail Transit, 2017(05):1-6.
[2]. Dong Junzhe, Yang Jianwei, Huang Qiang. Reliability Evaluation of Subway Vehicle Passenger Doors Based on GO Method [J]. Urban Rail Transit Research, 2013, 16(04):28-31+48.
[3]. Chen Hongyue, Hu Xuebing, Zhu Huidong, et al. Analysis of stress distribution characteristics in conveyor belts of belt conveyors [J]. Journal of Machine Design, 2020, 37(04): 55-60. (in Chinese)
[4]. Cao Zhongliang, Li Shan, Guo Jianhua. Dynamic load simulation analysis of syn-chronous belt drive based on MFBD [J]. Journal of Mechanical Transmission, 2016, 40(09): 142-144+149. (in Chinese)
[5]. Wang Zhengjie, Ge Zhenghao, Li Sen, et al. Research on dynamic performance of high-speed synchronous belt intermittent transmission device [J]. Packaging Engi-neering, 2018, 39(3): 172-177. (in Chinese)
[6]. Jozef Mascenik. The Influence of Changing Belt Loading Conditions on the Opera-tional Condition of the Belt Transmission [J]. Actuators, 2024, 13: 506.
[7]. Jiang Shaowei, Huang Wenquan. Dynamic simulation analysis of S3M synchronous belt for checkweigher based on RecurDyn [J]. Coal Mine Machinery, 2016, 37(04): 66-68. (in Chinese)
[8]. Ren Jihua, Huang Yunsheng, Zhao Yuncai. Research on transmission error and con-trol of polygon effect in synchronous pulley [J]. Coal Mine Machinery, 2017, 38(08): 37-39. (in Chinese)
[9]. Masataka Kagotani, Hiroshi Urata. Transmission Error Due to Resonance in Syn-chronous Belt Drive With Eccentric Pulley [J]. Journal of Mechanical Design, 2017, 139(12): 123301.
[10]. Bian Xianbing, Chen Zhiwei, Sun Xincheng, et al. Calculation and analysis of pol-ygon-like effect in non-circular synchronous belt drive (in English) [J]. Machine Tool & Hydraulics, 2020, 48(12): 10-16.